Dalton Transactions

ROYAL SOCIETY OF CHEMISTRY

PAPER

View Article Online
View Journal | View Issue

Cite this: *Dalton Trans.*, 2024, **53**, 2964

Expanding the library of sumanene molecular receptors for caesium-selective potentiometric sensors†

Joachim Ażgin, [a] Małgorzata Wesoły, [a] Krzysztof Durka, [a] Hidehiro Sakurai, [b,c] Wojciech Wróblewski [a] and Artur Kasprzak *[a]

Received 20th November 2023,
Accepted 8th January 2024

DOI: 10.1039/d3dt03885h

rsc.li/dalton

This paper reports the synthesis and characterization of eight sumanene molecular receptors for the selective recognition of caesium cations (Cs^+). The sumanene derivatives differed in the number (from one to nine), type (electron donating or electron withdrawing) and method of the attachment (functionalization of sumanene at the benzylic or aromatic carbons) of substituents in the sumanene skeleton. The ultimate goal of this work was to investigate the prospective use of various sumanene derivatives in the design of Cs^+-selective potentiometric sensors, thus, expanding the library of sumanene receptors for such applications. Spectroscopic fluorescence titration with caesium hexafluorophosphate revealed that the formation of sandwich complexes is highly favourable, but the steric hindrance of bulky substituents can disrupt this preference. In the case of triaryl-substituted sumanene derivatives, theoretical calculations show that, indeed, sandwich complexes are energetically more advantageous by 2.3 times than 1 : 1 complexes. Furthermore, such functionalization significantly increases receptor solubility in the polymeric membrane of the potentiometric sensors, which was quantitatively evaluated with the COSMO model.

Introduction

Sumanene (**1**, Fig. 1a) is a bowl-shaped fragment of fullerene C_{60} first synthesised by Sakurai, Daiko and Hirao in 2003,[1] attracting the attention of researchers in many fields ranging from basic structural studies to electroanalysis,[2–4] catalysis[5,6] and drug delivery.[7,8] Its unique physicochemical properties result from the presence of conjugated π–π bonds between carbon atoms allowing the formation of cation–π complexes. However, due to the bowl shape of sumanene molecules more than one binding site is available for cation complexation. The coordination properties of sumanene were first explored using theoretical calculations, which pointed out non-covalent Li^+ and Na^+ cation binding to both π-faces of a buckybowl by means of cation–π interactions.[9] More detailed computational studies on ion complexation to sumanene, considering the orientation and site of attack of metal ions, revealed that smaller Li^+ and Cu^+ ions prefer to bind to the convex surface of the rim 6-membered ring in the buckybowl, while the hub complexation of larger cations (Na^+, K^+) to the concave surface prevails.[10] The predicted values of interaction energy of sumanene with Li^+ in both its concave and convex positions corresponded well to those obtained in a later work.[11] Further theoretical studies on the nature of the cation–π interactions between chosen cations (Na^+, K^+, NH_4^+, tetramethylammonium, guanidinium, imidazolium) elucidated that a combination of electrostatic, induction and dispersion contributions controls the stability of the cation–π complexes.[12] In addition to the research on the interaction of cations with the sumanene molecule, dinitrogen bond cleavage by trimetallic clusters of sumanene with Ti, Zr, V and Nb was studied using DFT calculations.[5]

The most important result from the point of view of future inspirations of sumanene applications was the statement of formation of a sandwich-like complex with caesium cations *via* two sumanene molecules encapsulating the guest ion with their concave sites (see Fig. 1b). The driving force of this selective interaction was explained by a perfect size match of caesium cation (Cs^+) to sumanene bowl, which was experimentally proved using X-ray diffraction measurements of the

[a]*Faculty of Chemistry, Warsaw University of Technology, Noakowskiego Str. 3, 00-664 Warsaw, Poland. E-mail: artur.kasprzak@pw.edu.pl*
[b]*Division of Applied Chemistry, Graduate School of Engineering, Osaka University, 2-1 Yamadaoka, Suita, 565-0871 Osaka, Japan*
[c]*Innovative Catalysis Science Division, Institute for Open and Transdisciplinary Research Initiatives (ICS-OTRI), Osaka University, Suita, Osaka 565-0871, Japan*

†Electronic supplementary information (ESI) available: Compounds characterization data, data on spectroscopic studies, data on computational investigations. See DOI: https://doi.org/10.1039/d3dt03885h

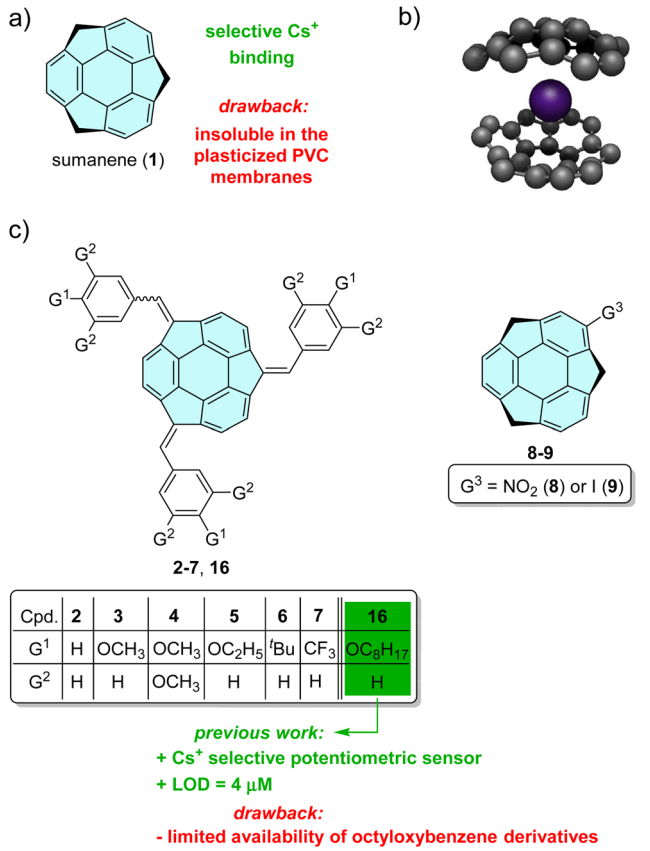

Fig. 1 (a) Structure of sumanene (**1**); (b) graphical representation of the possible structure of the sumanene–caesium complex; (c) structures of the investigated compounds **2–9**, together with the reference structure of *n*-octyloxybenzene sumanene derivative **16** and a graphical representation of the aims of this work in terms of the design of potentiometric sensors. Ref. 3 is related to our previous work on compound **16**.

complex of two sumanenyl monoanions and one caesium cation isolated under air-free conditions.[13] However, despite numerous theoretical and basic studies on sumanene cation–π complexes with alkali metal cations, there are only a few reports on the application of these compounds as molecular receptors.

The first report published in 2019 presented the synthesis of ferrocene-functionalized sumanenes, recognizing Cs^+ in the neutral state through cation–π interactions.[14] Spectroscopic studies revealed the 2 : 1 stoichiometry of the dynamically formed sandwich complex comprising one Cs^+ and two ferrocene-templated sumanene molecules. The sumanene–ferrocene derivatives were able to act as selective molecular receptors suitable for fluorescent[14,15] or electrochemical (namely amperometric)[2,4,16] sensors. Increasing the concentration of Cs^+ ions in sample solutions led to 'turn-off' fluorescence behaviour (lowering of the emission intensity)[15] or increase of the ferrocene oxidation current signal.[2,4,16] Further attempts were made to introduce a sumanene receptor into the membranes of potentiometric sensors – attractive analytical tools providing fast and selective measurements. However, the design of potentiometric sensors based on unmodified sumanene was difficult due to the insolubility of the receptor molecules in polymeric ion-selective membranes. Therefore, the synthesis of a sumanene derivative functionalized with *n*-octyloxybenzene moieties (compound **16**, Fig. 1c) was presented in the next report.[3] The receptor structure was tuned to enhance its solubility in the plasticized poly(vinyl chloride) (PVC) layer. The inspiration of this work was the structural similarity between compound **16** and *o*-nitrophenyl octyl ether (NPOE) widely used as a plasticizer of polymeric membranes. Potentiometric sensors based on polymer membranes doped with *n*-octyloxybenzene derivative **16** exhibited good selectivity and sensitivity towards Cs^+, with a detection limit of 4 μM. However, despite the encouraging results, in fact, only one derivative has been tested in such a device to date.

The aim of this work was to attempt to expand the library of molecular receptors suitable for potentiometric detection of Cs^+, simplifying the sumanene structure but still ensuring its (i) compatibility with polymeric PVC membranes, and (ii) Cs^+ recognition properties. Particular attention was paid to assess the impact of the electron donating and withdrawing groups, bound through a benzene ring (modification at the benzylic carbon) or directly (modification at the aromatic carbon) to the sumanene bowl (see Fig. 1b), on the Cs^+-selectivity of potentiometric sensors. Interactions between sumanene derivatives **2–9** and metal cations in solution were assessed spectroscopically using both UV–vis and fluorescence spectroscopy in order to estimate binding constants and investigate stoichiometry of dynamically formed complexes. The experimental part of the studies was also supported by quantum mechanical calculations. These were performed to shed light on the nature of sumanene–Cs^+ interactions, in particular, to estimate the interaction energy between the sumanene derivatives and caesium, predict and interpret UV–vis spectra and compute solvation energy of the sumanene derivatives in ion-selective membranes.

Experimental section

Materials and methods

Chemical reagents and solvents for the synthesis were commercially purchased and purified according to the standard methods, if necessary. All inorganic salts were of analytical grade and were purchased from Fluka. The solutions of inorganic salts (0.01 M) were prepared with deionised water. High-molecular-weight poly(vinyl chloride) (PVC), *o*-nitrophenyl octyl ether (*o*-NPOE), and potassium tetrakis[3,5-bis(trifluoromethyl)phenyl]borate (KTFPB) were obtained from Fluka (Selectophore). Freshly distilled tetrahydrofuran (THF, Fluka) was used as a solvent for membrane components.

Thin layer chromatography (TLC) and preparative thin layer chromatography (PTLC) were performed using Merck Silica gel 60 F254 plates.

NMR experiments were carried out using a Varian VNMRS 500 MHz spectrometer (^1H at 500 MHz, $\{^1H\}^{13}C$ NMR at

125 MHz) equipped with a multinuclear *z*-gradient inverse probe head. The spectra were recorded at 25 °C and standard 5 mm NMR tubes were used. ^{1}H and ^{13}C chemical shifts (δ) were reported in parts per million (ppm) relative to the solvent signal, *i.e.*, $CDCl_3$: δ_H (residual $CHCl_3$) 7.26 ppm and δ_C (residual $CHCl_3$) 77.16 ppm. In the case of NMR, spectra were analyzed with the MestReNova v12.0 software (Mestrelab Research S.L.). ESI-HRMS (TOF) measurements were performed with a Q-Exactive Thermo Scientific spectrometer.

Syntheses

The syntheses of sumanene (**1**),[1] (tris((phenyl)methidene) sumanene) **2**,[17] (tris((4-methoxyphenyl)methidene)sumanene) **3**,[17] (tris((3,4,5-trimethoxyphenyl)methidene)-sumanene) **4**,[17] (tris((4-trifluoromethylphenyl)methidene)sumanene) **7**,[17] 2-nitrosumanene[18] and 2-iodosumanene **9**[4] are described elsewhere.

General method for the synthesis of (tris((4-triethoxyphenyl) methidene)sumanene) 5 and (tris((4-*tert*-butylphenyl) methidene)sumanene) 6

Sumanene (**1**; 15.0 mg, 0.057 mmol, 1 equiv.) was placed in a reaction test tube. To this, tetrabutylammonium bromide (TBAB; 9.2 mg, 0.0285 mmol, 0.5 equiv.) was added. THF (0.2 mL) and $NaOH_{aq}$ (30%, 2 mL) were then added, and the reaction mixture was stirred for several minutes at room temperature. Aldehyde (**13** and **14**; 6 equiv.) was added in one portion. The reaction mixture was stirred for 48 hours at room temperature. Distilled water (6 mL) was added. The crude product was extracted with CH_2Cl_2 (3 × 20 mL). Organic layers were combined, washed with saturated NH_4Cl, water, and brine. After drying with $MgSO_4$ followed by filtration, volatiles were distilled off using a rotary evaporator. Finally, the product was purified using preparative thin layer chromatography (PTLC) to obtain the target compounds **5** and **6**.

Compound 5. Orange solid. Yield 50% (18.9 mg). ^{1}H NMR ($CDCl_3$, 500 MHz, ppm) δ_H 7.88–7.84 (m, 3H), 7.81–7.78 (m, 3H), 7.50–7.48 (m, 1.5H), 7.36–7.31 (m, 4H), 7.27–7.26 (m, 2H), 7.16–7.13 (m, 1.5H), 7.01–6.93 (m, 6H), 4.16–4.07 (m, 6H), 1.50–1.44 (m, 9H). $\{^{1}H\}^{13}$C NMR ($CDCl_3$; 125 MHz, ppm) δ_C 159.7 × 2, 159.6, 147.9, 147.5 × 2, 147.4, 147.2, 147.1, 146.0, 145.6, 145.4, 145.1 × 2, 143.3, 143.0, 141.4, 141.1, 139.0 × 2, 138.9 × 2, 131.4 × 3, 131.3, 128.9, 128.8 × 2, 128.7, 128.4, 128.1 × 2, 127.8, 123.4, 123.3, 123.2, 123.0, 120.7, 120.6, 120.5, 120.4, 114.7 × 2, 63.7 × 2, 15.0 × 2. HRMS (ESI) *m*/*z* $[M + H]^+$ calcd for $C_{48}H_{37}O_3$ 661.27372, found 661.27389. R_f (40% hex./CH_2Cl_2) = 0.56.

Compound 6. Orange solid. Yield 90% (35.8 mg). ^{1}H NMR ($CDCl_3$, 500 MHz, ppm) δ_H 7.89–7.79 (m, 6H), 7.53–7.49 (m, 4H), 7.47–7.44 (m, 3.5H), 7.41–7.38 (m, 3H), 7.36–7.34 (m, 3H), 7.20–7.17 (m, 1.5H), 1.41–1.37 (m, 27H). $\{^{1}H\}^{13}$C NMR ($CDCl_3$; 125 MHz, ppm) δ_C 152.2 × 3, 152.1, 149.1, 148.9, 148.0, 147.7, 147.6 × 2, 147.3 × 2, 146.2, 145.8, 145.6 × 2, 145.3, 143.4, 143.2, 141.6, 141.4, 140.0 × 2, 139.9, 133.6, 133.5 × 2, 133.4, 129.7, 129.6, 128.6, 128.4, 128.3, 128.1, 125.8, 125.7, 123.7, 123.5, 123.4 × 2, 120.9, 120.8 × 2, 120.6, 31.5, 31.4. HRMS (ESI) *m*/*z* $[M + H]^+$ calcd for $C_{54}H_{49}$ 697.38288, found 697.38276. R_f (1% $CH_3OH/CHCl_3$) = 0.68.

Sensor preparation and EMF measurements

The method of membrane and sensor preparation was the same as that for standard ion-selective electrodes. The membranes contained 1 wt% sumanene derivatives **2–9**, 65 wt% plasticizer, 33 wt% PVC and 5–70 mol% (*vs.* receptor) KTFPB. Membrane components (200 mg in total) were dissolved in 1.5 mL of THF. The solution was poured into a glass ring placed on a glass plate. After solvent evaporation, membrane discs of appropriate size were cut off and mounted in electrode bodies (Type IS 561, Philips) for electromotive force (EMF) measurements. NaCl solution (0.01 M) was used as an internal filling; the electrodes were conditioned overnight in CsCl solution (0.01 M). For each membrane composition three sensor specimens were prepared.

All measurements were carried out with cells of the following type: Ag, AgCl; KCl 1 M/CH_3COOLi 1 M/sample solution// membrane//internal filling solution; AgCl, Ag.

A potentiometric multiplexer (EMF 16 Interface, Lawson Labs Inc., Malvern, USA) was used for the EMF measurements. The values of the potentiometric selectivity coefficients ($\log K_{Cs,X}$) of the ion-selective electrodes were determined by the separate solution method (SSM) using 0.01 M solutions of nitrate salts.[19,20] The calibration curves of the sensors were examined by measuring the EMFs in 0.01 M solution of sodium nitrate, increasing the activity of the Cs^+ in steps of 0.5 $\log a$ (concentration range $10^{-6.5}$ to 10^{-1} M), pH 7.0. The activities of ions in the aqueous solutions were calculated according to the Debye–Hückel approximation.

Theoretical calculations

Calculations with NWChem[21] were carried out using the plane-wave pseudopotential method (PSPW) with a simulation cell of 100 Å (for tris-substituted sumanene derivatives) or 20 Å (for mono-substituted sumanene derivatives) and energy cutoff of 15 Hartree, using Vosko exchange correlation potential. Initial geometries were prepared in Avogadro molecular editor[23,24] based on the geometry from the crystal structure of sumanene.[25] Then, molecules were subjected to an optimization procedure in NWChem. Following geometry optimization, the vibrational frequencies were calculated and the results showed that optimized structures are stable geometric structures (no imaginary frequencies). In the optimization processes no symmetry constraints were applied. The geometries of optimized structures are given in the ESI (Tables S3–S16†). Solvation energies were computed using the conductor-like screening model (COSMO).[26]

Computations using Gaussian[22] software were performed in order to simulate the UV–vis spectrum of compound **3**. The B3LYP functional (DFT)[27] with 6-311++G(d,p)[28] basis set was applied to optimize ground state geometry. Then vertical excitation energies were obtained using the TD-DFT method at the same level of theory. The energy values of six lowest singlet excited states are presented in Fig. 4. Because the TD-DFT cal-

culations showed that the excitation involved mixed molecular orbitals, we employed natural transition orbitals (NTOs)[29] in order to visualize active vertical excitation (S_1/S_2 and S_5/S_6 states). The NTOs provide a quantitative and more intuitive description of the electronic excitation with the highest occupied NTO (HONTO) and the lowest unoccupied NTO (LUNTO) representing the distributions of holes and electrons, respectively. The NTOs were visualized with the Avogadro molecular editor.

Spectroscopic studies

The UV–vis absorption spectra were recorded using an Agilent Technologies Carry 60 UV–vis spectrometer with scanning speed of 600 nm min^{-1} and 2 nm slits using Starna scientific quartz cuvettes (10.00 mm). Emission spectra were recorded with a HITACHI F-7100 FL spectrometer, with scanning speed of 240 nm min^{-1}, delay of 0.0 s, EX slit of 5.0 nm, EM slit of 5.0 nm, and PMT voltage of 400 V. The measurements were performed at room temperature. To eliminate any background emission, a spectrum of pure solvent was subtracted from the samples' spectra. Fluorescence measurements were carried out with excitation at the wavelength of absorption maximum.

Stock solutions of sumanene derivatives were prepared by dissolving weighed amounts of sumanene derivative in THF to yield a solution concentration of 2×10^{-4} M. Solutions used for measurements were prepared by diluting stock solution with THF and then water to yield a final concentration of sumanene derivative equal to 2×10^{-5} M. The resultant solvent system used for these analyses was 50 vol% water in THF. Each titration experiment consisted of 9 steps. First, absorbance or fluorescence of a solution containing only a sumanene derivative was measured, then Cs^+ salts dissolved in water were added in 8 consecutive steps to achieve the following proportions of Cs^+ to sumanene: 0.001., 0.005., 0.01., 0.05., 1., 2., 5. and 10 eq. To ensure proper mixing, a magnetic stir bar was placed in a cuvette. After placing the cuvette in a spectrometer, a small permanent magnet was mounted on the side of the cuvette to hold the magnetic stir bar out of the light beam to prevent it from interfering with the light source.

Results and discussion

Synthesis

Tris-substituted sumanene derivatives **2–7** were obtained by means of the condensation-type reaction[17] employing sumanene (**1**) and benzaldehyde derivatives (**10–15**) as starting materials (Scheme 1). The reaction was performed under phase-transfer catalysis (PTC) conditions in the water–tetrahydrofuran (THF) solvent system. A 30% aqueous solution of NaOH was employed as a base, while tetrabutylammonium bromide (TBAB) was used as a PTC catalyst. Reactions were performed at room temperature for 24–48 hours. In the case of compounds **2**, **3**, **5** and **7**, the product was purified using column chromatography. The purification of compounds **4** and **6** required two-steps, firstly by column chromatography

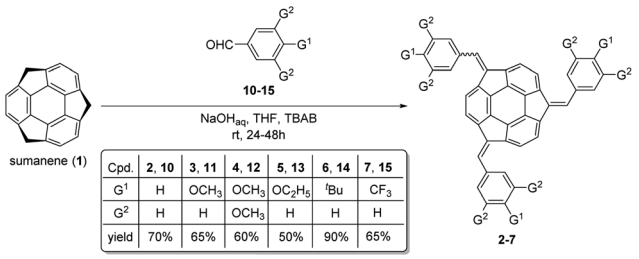

Cpd.	2, 10	3, 11	4, 12	5, 13	6, 14	7, 15
G^1	H	OCH_3	OCH_3	OC_2H_5	^{t}Bu	CF_3
G^2	H	H	OCH_3	H	H	H
yield	70%	65%	60%	50%	90%	65%

Scheme 1 Synthesis of tris-substituted sumanene derivatives **2–7**.

followed by preparative thin-layer chromatography (PTLC). Synthesis of mono-substituted sumanene derivatives **8** and **9** (Scheme 2) employed the electrophilic aromatic substitution (S_EAr) reaction.[4,18] 2-Nitrosumanene **8** was obtained (60%) by treating sumanene **1** with nitric acid in the presence of trifluoroacetic acid anhydride (TFAA) at −20 °C. Monoiodination of sumanene was performed using 1,3-diiodo-5,5-dimethylhydantoin in the presence of triflic acid (TfOH), yielding 2-iodosumanene **9** (85%).

Compounds **2–9** were analysed using NMR spectroscopy and high-resolution mass spectrometry (HRMS). While **2–4** and **7–9** are known compounds,[17,18] compounds **5** (tris((4-ethoxyphenyl)methidene)sumanene) and **6** (tris((4-*tert*-butylphenyl)methidene)-sumanene) had not been synthesized before. Copies of the spectra of **5** and **6** are presented in Fig. S1–S9 in the ESI.† Similar to the spectra of other tris-substituted sumanene derivatives,[3,16,17] the spectra of **5** and **6** comprised the signals of two diastereoisomers, namely C_3-symmetrical and unsymmetrical. The major factors in the NMR spectra that confirmed the successful synthesis of **5** and **6** were (i) the changes in the profiles of signals in the aromatic region, (ii) the lack of signals coming from the benzylic protons of the sumanene skeleton, and (iii) the presence of signals coming from the substituent in the phenylene ring. The HRMS spectra ultimately confirmed that compounds **5** and **6** were obtained.

Potentiometric experiments

Sumanene derivatives **2–9** were introduced into PVC/*o*-NPOE membranes, used commonly as receptor layers of ion-selective

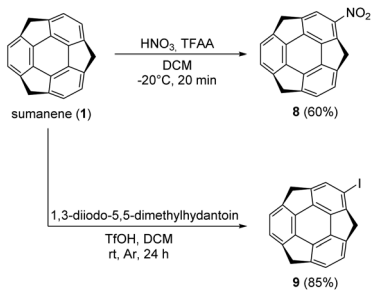

Scheme 2 Synthesis of mono-substituted sumanene derivatives **8** and **9**.

Table 1 Values of selectivity coefficients ($\log K_{Cs,X}$) of potentiometric sensors formulated with sumanene derivatives **2–9** (20 mol% KTFPB) and without sumanene receptor (blank membrane) in PVC/*o*-NPOE membranes (mean values calculated for 3 electrode specimens). Selectivity coefficients of ion-selective electrodes based on octyloxybenzene sumanene derivative **16** [3] are also presented for comparison

	$\log K_{Cs,Li}$	$\log K_{Cs,Na}$	$\log K_{Cs,K}$	$\log K_{Cs,NH_4}$	$\log K_{Cs,Rb}$	$\log K_{Cs,Ba}$	$\log K_{Cs,Ca}$
Blank	−3.30	−2.50	−1.00	−1.50	−0.50	−3.50	−3.80
2	−3.60	−2.90	−1.30	−1.65	−0.60	−2.60	−2.85
3	−3.20	−2.70	−1.25	−1.55	−0.55	−3.30	−3.60
4	−3.30	−2.60	−1.05	−1.45	−0.50	−2.90	−3.55
5	−3.40	−3.00	−1.35	−1.75	−0.60	−3.20	−4.00
6	−3.40	−3.20	−1.45	−1.80	−0.60	−3.40	−4.00
7	−3.40	−2.75	−1.20	−1.60	−0.55	−2.95	−3.05
8	−3.70	−3.00	−1.10	−1.55	−0.50	−2.40	−2.70
9	−3.80	−3.15	−1.20	−1.60	−0.55	−2.50	−2.80
16 [3]	—	−3.10	−1.50	−1.80	−0.70	−3.70	−4.10

electrodes. The selectivity of ion binding by the studied derivatives was evaluated on the basis of potentiometric selectivity coefficients (Table 1), expressing quantitatively the influence of a given interfering ion on the signal of the ion-selective electrode sensitive towards the Cs^+ cation. The values of selectivity coefficients have been determined against the most relevant interfering cations in a heterogeneous system (polymeric membrane/water solution), which means that all derivatives were soluble in the PVC/*o*-NPOE membranes (limited solubility was observed only for receptors **7** and **8**).

Polymeric membranes based on sumanene derivatives **2–9** exhibited enhanced selectivity towards the Cs^+ cation against alkali and alkaline earth metal cations in comparison with the membranes containing only the lipophilic salt KTFPB (blank membranes), presenting the cation-selectivity following the so-called Hofmeister sequence[19,20] (comparison with the selectivity of exemplary receptors reported in the literature is included in the ESI†). Although all sensors showed similar selectivity patterns (with a strong interference from rubidium cations), some differences in cation binding by the tested derivatives can be noticed. The membranes based on the most lipophilic receptor **6** (with *tert*-butyl substituents) provided the highest caesium selectivity (*i.e.*, the lowest values of $\log K_{Cs,X}$), whereas the presence of oxygen atoms in the receptor structure suppressed this preference. The most pronounced effect was observed for the derivative **4** with three methoxy groups – its introduction into the membrane did not alter the selectivity pattern of blank membranes. This can be explained by the competitive cation binding by the adjacent methoxy groups against the selective cation–π interactions between the sumanene bowl and Cs^+, resulting in a loss of membrane caesium selectivity (the selectivity is governed by the KTFPB ion-exchanger). On the other hand, the elongation of the alkyl chain in methoxy-, ethoxy-, and octyloxybenzene series favorably influenced the selective recognition of Cs^+. Finally, it should be emphasized that the electron donating or withdrawing properties of the substituents bound in various positions did not correlate with the selectivity of membranes based on receptors **2–6** and **7–9**, respectively. This result indicates that the ion binding selectivity is mainly due to the interactions of the cations with the sumanene bowl.

According to our previous results, a lipophilic anionic additive (KTFPB) was added to the membrane based on sumanene derivatives (neutral carriers) to provide proper operation of the sensors and reduce the interferences from lipophilic anions.[30,31] Different amounts of the KTFPB lipophilic salt were tested, since appropriately tuned concentrations of ionic sites can improve the membrane selectivity.[30,31] However, during our studies comparable values of selectivity coefficients were obtained, changing the amount of KTFPB lipophilic salt in the membrane in the range 5–70 mol% *vs.* the receptor (exemplary selectivity patterns of membranes formulated with receptor **3** and various KTFPB amounts were collected and are shown in Table S1, ESI†). Moreover, similar values of selectivity coefficients of membranes containing 40% and 70 mol% KTFPB suggest that sumanene : Cs^+ complexes of 2 : 1 but also 1 : 1 stoichiometry could be formed in the polymeric phase.

Caesium response curves of the ion-selective electrodes with membranes doped with sumanene derivatives **2–9**, determined in 0.01 M $NaNO_3$ solution, exhibited quite a wide linear range, at least from 28 μM to 3 mM Cs^+ (Fig. 2). The slopes of the calibration curves slightly depended on the structure of the sumanene derivative introduced into the membrane. The highest sensitivity towards the target Cs^+ cations, *i.e.*, 51.0–53.5 mV dec^{-1} (with a detection limit of 5.6 μM Cs^+) was measured for the sensors based on receptors **5** and **6**, whereas lower slope values were found for the other ion-selective electrodes (47.0–50.5 mV dec^{-1}, detection limit 8.9 μM Cs^+). All constructed ion-selective electrodes were characterized by a short response time of 120–180 s (see Fig. S11, ESI†).

Spectroscopic experiments

Supramolecular interactions between the sumanene derivatives and Cs^+ were further studied using UV-vis absorption and fluorescence spectroscopy. For these studies, two triaryl-substituted derivatives functionalized with the methoxy (**3**) or *tert*-butyl (**6**) groups and one mono-substituted derivative, namely 2-iodosumanene (**9**), were selected. The selection of these systems was rationalized by their diverse molecular structures and good affinity towards Cs^+ cations. Note that due to the limited solubility of the sumanene derivatives in water, the organic solvent additive was necessary to conduct the spectro-

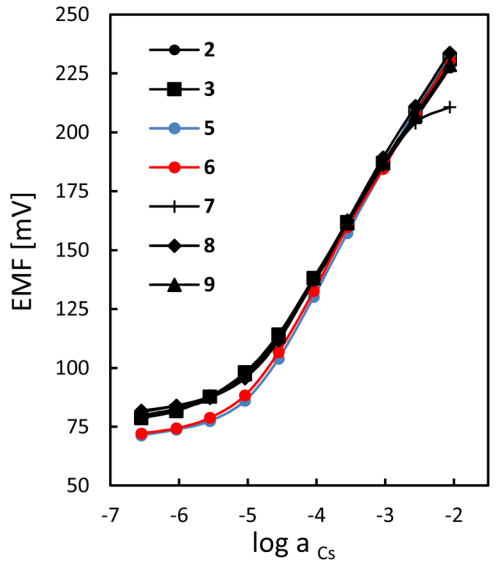

Fig. 2 Potentiometric responses of sensors formulated with sumanene derivatives **2–9** (20 mol% KTFPB, PVC/*o*-NPOE) towards caesium cations measured in 0.01 M $NaNO_3$ solution (for the sake of clarity the calibration curve of the ion-selective electrode based on membranes doped with sumanene derivative **4** is not presented).

scopic experiments at reasonable concentration ranges. Therefore, 1 : 1 vol : vol THF and water mixture was selected.

At first, the UV-vis spectra of native compounds **3**, **6** and **9** were measured. Compounds **3** and **6** exhibited similar spectral features with three distinct absorption bands at *ca.* 240, 360 and 470 nm (see Fig. S12 in the ESI†). The highest energy band can be attributed to the electron transition within the central sumanene unit,[17] while the two remaining bands resulted from the delocalization of the π-electron density on the adjacent phenyl units. Both long-wavelength absorption bands disappeared in **9**, while the short-wavelength band was bathochromically shifted to 270 nm (see Fig. S12 in the ESI†). The emission spectra show one maximum at 530 nm (for **3** and **6**) and at 380 nm (for **9**), which are independent on the excitation wavelength in agreement with Kasha's rule.

In the initial phase of the studies on supramolecular interactions between selected sumanene derivatives and Cs^+, a series of UV-vis titrations for representative compound **3** were performed using various caesium salts, namely, hexafluorophosphate, nitrate, fluoride, chloride, sulphate(VI) and carbonate (titration curves of compound **3** with different caesium salts are presented in Fig. S13 in the ESI†). Upon the addition of caesium salt, the intensity of the longest-wavelength absorption band systematically decreased. Acquired data were further analysed using Job's plot method to determine stoichiometry of the **3**:Cs^+ complex and the Benesi–Hildebrand method[32] was used to estimate the apparent binding constant. The most reliable results (K_{app} = 7 × 10^6 M^{-2}, complex stoichiometry 2 : 1) were obtained for caesium hexafluorophosphate ($CsPF_6$), whereas the analysis of the titration data for caesium nitrate, chloride and sulphate(VI) led to inconclusive results. For this reason, further titration experiments were carried out with $CsPF_6$.

Because the UV-vis method was found to have sensitivity that is too low for the studied system, further studies were carried out using fluorescence spectroscopy (emission spectra of the sumanene derivatives **3**, **6** and **9** are presented in Fig. S14 in the ESI†). Fluorescence titration experiments were carried out using the same protocol as for the UV-vis titrations. As in the case of the UV-vis absorption spectra, the fluorescence signal (λ_{em} = 535 nm) systematically decreased with the addition of Cs^+ (see the spectra for the representative compound **6**, Fig. 3). According to our results, compounds **3** and **9** formed 2 : 1 sandwich complexes with Cs^+ in similar manner to unsubstituted sumanene (Table 2). In contrast, *tert*-butyl derivative **6** formed a 1 : 1 complex with Cs^+. The reduced preference for the formation of sandwich complexes can be explained by steric hindrance of the bulky *tert*-butyl groups hampering the approximation of two sumanene units from the concave sites. Compounds **3** and **6** had similar apparent binding constants (K_{app}) towards Cs^+ (K_{app} = 6–7 × 10^6 M^{-2}). However, in the case of 2-iodosumanene (**9**), a significantly lower binding constant was observed despite its similar selectivity towards Cs^+ derived from the potentiometric experiments.

Finally, the interactions of the representative sumanene derivative **3** with lithium cations (Li^+) were investigated using

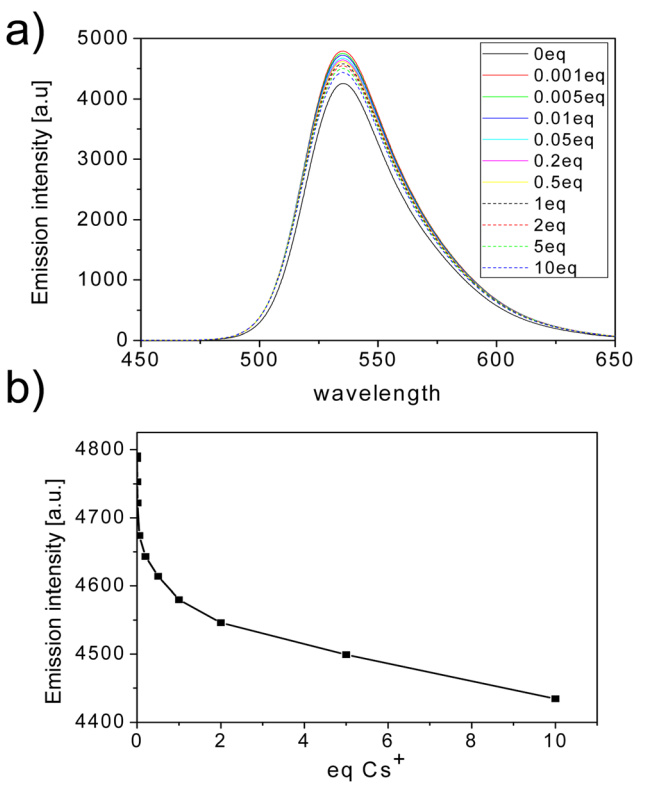

Fig. 3 (a) Fluorescence Cs^+ titration of representative compound **6** (λ_{ex} = 365 nm; the legend denotes the eq. value of Cs^+ added). (b) Graph representing the results of the fluorescence titration of compound **6** with Cs^+ (data for λ_{em} = 535 nm).

Table 2 Summary of binding parameters and binding stoichiometries (both estimated from fluorescence titration) for non-covalent systems formed of Cs^+ with **3**, **6** or **9**

Compound	K_{app} [10^4 M^{-2}]	Sumanene derivative:Cs^+
3	735	2 : 1
6	624	1 : 1
9	91	2 : 1

fluorescence spectroscopy. Following the previously described procedures, **3** was titrated with lithium hexafluorophosphate and the fluorescence spectra were recorded (λ_{ex} = 350 nm, see Fig. S15 in the ESI†). The obtained results allowed for the estimation of the apparent binding constant of lithium using the Benesi–Hildebrand method that was found to be equal to 12 × 10^4 M^{-2}. This value is significantly lower than the apparent binding constant of Cs^+, which stays in agreement with observed selectivity during the potentiometric measurements.

Theoretical calculations

This part of the study was performed with quantum mechanical calculations using the plane-wave pseudopotential method (PWPM) with NWChem software or the FT method with the Gaussian program package. Calculations were aimed at the following goals: (i) prediction and interpretation of the UV-vis spectra of the sumanene derivatives using the TD-DFT method; (ii) calculation of the interaction energy between the sumanene derivatives and caesium ions to assess the impact of structure modification on the coordination properties of the investigated compounds; and (iii) the prediction of the solubility of the sumanene derivatives in potentiometric membranes by computing the solvation energy using the COSMO solvation model. The triphenyl-substituted sumanene (**2**), serving as the model compound without any substituents present in the introduced phenyl rings, and the sumanene monosubstituted with the electron withdrawing group, namely 2-nitrosumanene (**8**), were added to the spectroscopically studied sumanene derivatives **3**, **6** and **9**.

At first, the UV-vis absorption spectra of two diastereoisomers of compound **3** (C_3-symmetrical and unsymmetrical)[17] were predicted using the TD-DFT method with the B3LYP functional. Computed spectra are generally in good agreement with the experimentally obtained spectrum (see Fig. S16 in the ESI†). According to our calculations, the two lowest energy levels S_1 and S_2 are degenerate and correspond to the highest absorption wavelength on the UV-vis spectrum at λ = 472 nm. Higher energy levels S_5 and S_6 are also nearly degenerate and correspond to the absorption at λ = 383 nm, while the S_3 and S_4 energy levels are not populated due to the small oscillator strength value. In addition, the higher intensity of the peak at 383 nm can possibly be explained by the higher molar absorption coefficient of symmetric isomers. Following the absorption spectrum prediction, natural transition orbitals (NTOs) were computed in order to study the nature of particular electronic transitions. The distribution of HONTO and LUNTO pairs for the S_1 and S_5 states are presented along with the energy level diagram in Fig. 4. The HONTO pairs are generally identical for both states and they are spread over the centre of a molecule and two out of the three aromatic rings attached to the sumanene moiety. For the S_1 state configuration, the LUNTO is delocalised on the whole molecule, whereas for S_5 it is distributed in a similar region as the HONTO. Thus, the formation of two different absorption bands can be rationalized in terms of the delocalization of the LUNTO, which is naturally more effective for the lower energy state.

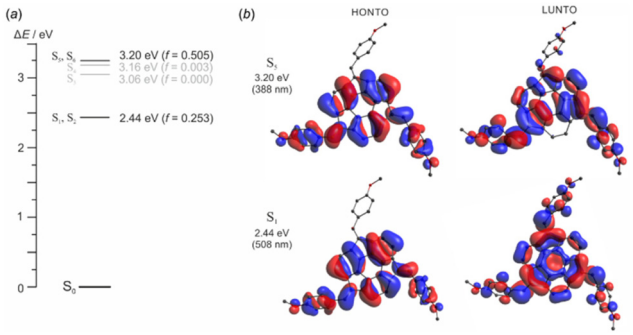

Fig. 4 (a) Energy diagram and (b) natural transition orbitals of compound **3**.

In the next step, the interaction energies between sumanene (**1**) and its derivatives **2**, **3**, **8** and **9** and Cs^+ were evaluated (Fig. 5b). First, the interaction energies were computed for three different modes of binding: Cs^+ bonded in the concave and the convex site, and the sandwich complex of two sumanene molecules with one Cs^+ located at the concave site (see Fig. 5a for the structures of the considered Cs^+ complexes presented representatively for the sumanene molecule).

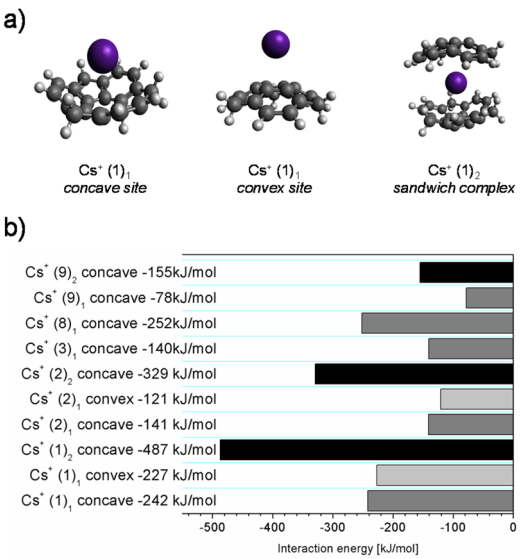

Fig. 5 (a) Structures representing possible sumanene:Cs^+ binding modes. (b) Computed binding energies of caesium to selected sumanene derivatives.

According to expectations, binding of Cs^+ at the concave site is energetically more favoured than binding at the convex site. Furthermore, sandwich complex $(\mathbf{1})_2$:Cs^+ exhibits an interaction energy that is two times larger than that of the sumanene molecule **1**:Cs^+ complex. This fact agrees with the results obtained for the complex of two sumanene anions and Cs^+.[13] Interestingly, the interaction energy of derivative **2** with Cs^+ is 2.3 times larger for the sandwich complex than it is for the 1 : 1 complex. The net energy gain comes from the attraction between neighbouring aromatic rings located at the benzylic positions of two sumanene molecules from the complex.

Taking into consideration 1 : 1 complexes, native sumanene **1** exhibits a significantly higher interaction energy with Cs^+ than its derivatives, with the exception of 2-nitrosumanene **8**, which is characterized by the highest stability among the studied series. The high interaction energy of 2-nitrosumanene **8** with Cs^+ correlates with its good performance observed during the potentiometric measurements. In contrast, 2-iodosumanene **9** exhibits the lowest interaction energy (for the 1 : 1 complex) of all the investigated sumanene derivatives, which is also in agreement with its significantly lower apparent binding constant observed during the spectroscopic measurements. In the case of tris-arylated derivatives **2** and **3**, their very similar complexation energies are consistent with the comparable selectivity of the respective potentiometric sensors.

Finally, the solvation energies of the studied sumanene receptors in the *o*-NPOE plasticizer were calculated to elucidate the impact of the ligand structure on its solubility in the membrane phase. According to the results of our previous studies, the unmodified sumanene **1** crystallized in the PVC/*o*-NPOE membrane, whereas good solubility of derivatives **2–9** provided proper functioning of the potentiometric sensors (a limited solubility was observed only for **7** and **8**). To dissolve the given compound, its energy of interaction with the solvent has to overcome the crystal lattice energy. Unfortunately, due to a lack of crystal structural data, free energies of solvation (in the thermodynamic sense) could not be strictly evaluated. For this reason, only the energies of interaction between the sumanene derivatives and the plasticizer were computed. The solvation energies obtained with the COSMO model correlate well with the experimental solubility data and the observed receptor solubilities in the plasticized PVC (Table S2, ESI†) for all the investigated sumanene derivatives (except for 2-iodosumanene **9**, which is soluble in an ion-selective membrane, but computations yielded low solvation energy). Moreover, significant differences were observed between the unmodified and mono- or tri-substituted receptors. This result indicates that the presence of aromatic substituents ensured good solubility in the membrane phase, whereas further functionalization with alkyl chains only slightly affects the solubility. On the other hand, comparable values of solvation energy calculated for the insoluble sumanene **1** and the soluble 2-iodosumanene derivative **9** can be explained by possible halogen interactions between 2-iodosumanene and poly(vinyl chloride), which are not considered by the COSMO solvation model that accounts only for electrostatic interactions.

Conclusions

In conclusion, the synthesis, characterization and application of eight sumanene derivatives (**2–9**) as molecular receptors in Cs^+-selective potentiometric sensors were investigated. The results obtained in this work demonstrated that the simplified structure of the receptor molecules ensures satisfactory analytical performance of the constructed sensors, even compared to the previously developed device based on *n*-octyloxybenzene sumanene.[3] Moreover, the simplified receptor structure, compatible with PVC membranes, can be easily functionalized to tune the receptor affinity towards other analytes. Notably, computed solvation energies using the COSMO model on the interactions between the sumanene derivatives and the plasticizer correlate well with experimental solubility data and the observed receptor solubilities in the plasticized PVC. Selective action of the sumanene derivatives towards detection of Cs^+ was also confirmed spectroscopically and by using theoretical calculations. The computed interaction energies between the sumanene derivatives and Cs^+ were in good agreement with results of spectroscopic measurements, *i.e.*, compounds with higher binding constants (estimated from spectrofluorimetric titration) exhibited larger computed interaction energies. We believe this work expands the knowledge on the design of sumanene-containing analytical tools for Cs^+ detection, as well as the general understanding on the nature of sumanene–Cs^+ interactions.

Conflicts of interest

There are no conflicts to declare.

Acknowledgements

The financial support from the National Science Centre, Poland, OPUS grant no. 2021/43/B/ST4/00114 (A. K.) and Warsaw University of Technology (WUT), as well as JSPS KAKENHI (grant no. JP19H00912 and JP21H05233; H. S.), is acknowledged. This research was carried out with the support of the Interdisciplinary Centre for Mathematical and Computational Modelling, University of Warsaw (ICM UW) under computational allocation no G91-1416.

References

1 H. Sakurai, T. Daiko and T. Hirao, *Science*, 2003, **301**, 1878–1878.
2 A. Kasprzak, A. Kowalczyk, A. Jagielska, B. Wagner, A. M. Nowicka and H. Sakurai, *Dalton Trans.*, 2020, **49**, 9965–9971.
3 A. Kasprzak, A. Tobolska, H. Sakurai and W. Wróblewski, *Dalton Trans.*, 2022, **51**, 468–472.

4 A. Kasprzak, A. Gajda-Walczak, A. Kowalczyk, B. Wagner, A. M. Nowicka, M. Nishimoto, M. Koszytkowska-Stawińska and H. Sakurai, *J. Org. Chem.*, 2023, **88**, 4199–4208.
5 Y.-Y. Wang, X.-L. Ding, Y. Chen, M.-M. Wang, W. Li and X. Wang, *Phys. Chem. Chem. Phys.*, 2022, **24**, 23265–23278.
6 T. Thiruppathiraja, A. L. Arokiyanathan and S. Lakshmipathi, *Fuel Cells*, 2021, **21**, 490–501.
7 J. S. Al-Otaibi, Y. S. Mary, Y. S. Mary, A. Mondal, N. Acharjee and D. G. Churchill, *Comput. Theor. Chem.*, 2022, **1215**, 113811.
8 M. Nezamabadi, E. Balali and M. Qomi, *Inorg. Chem. Commun.*, 2023, **155**, 111098.
9 U. D. Priyakumar and G. N. Sastry, *Tetrahedron Lett.*, 2003, **44**, 6043–6046.
10 D. Vijay, H. Sakurai, V. Subramanian and G. N. Sastry, *Phys. Chem. Chem. Phys.*, 2012, **14**, 3057.
11 I. K. Petrushenko, N. V. Shipitsin and K. B. Petrushenko, *Phys. E*, 2022, **135**, 114949.
12 J. A. Carrazana-García, E. M. Cabaleiro-Lago and J. Rodríguez-Otero, *Phys. Chem. Chem. Phys.*, 2017, **19**, 10543–10553.
13 S. N. Spisak, Z. Wei, A. Yu. Rogachev, T. Amaya, T. Hirao and M. A. Petrukhina, *Angew. Chem., Int. Ed.*, 2017, **56**, 2582–2587.
14 A. Kasprzak and H. Sakurai, *Dalton Trans.*, 2019, **48**, 17147–17152.
15 A. Kasprzak and H. Sakurai, *Chem. Commun.*, 2021, **57**, 343–346.
16 J. S. Cyniak, Ł. Kocobolska, N. Bojdecka, A. Gajda-Walczak, A. Kowalczyk, B. Wagner, A. M. Nowicka, H. Sakurai and A. Kasprzak, *Dalton Trans.*, 2023, **52**, 3137–3147.
17 T. Amaya, K. Mori, H.-L. Wu, S. Ishida, J. Nakamura, K. Murata and T. Hirao, *Chem. Commun.*, 2007, 1902–1904.
18 B. B. Shrestha, S. Karanjit, G. Panda, S. Higashibayashi and H. Sakurai, *Chem. Lett.*, 2013, **42**, 386–388.
19 E. Bakker, P. Bühlmann and E. Pretsch, *Chem. Rev.*, 1997, **97**, 3083–3132.
20 P. Bühlmann, E. Pretsch and E. Bakker, *Chem. Rev.*, 1998, **98**, 1593–1688.
21 E. Aprà, E. J. Bylaska, W. A. De Jong, N. Govind, K. Kowalski, T. P. Straatsma, M. Valiev, H. J. J. Van Dam, Y. Alexeev, J. Anchell, V. Anisimov, F. W. Aquino, R. Atta-Fynn, J. Autschbach, N. P. Bauman, J. C. Becca, D. E. Bernholdt, K. Bhaskaran-Nair, S. Bogatko, P. Borowski, J. Boschen, J. Brabec, A. Bruner, E. Cauët, Y. Chen, G. N. Chuev, C. J. Cramer, J. Daily, M. J. O. Deegan, T. H. Dunning, M. Dupuis, K. G. Dyall, G. I. Fann, S. A. Fischer, A. Fonari, H. Früchtl, L. Gagliardi, J. Garza, N. Gawande, S. Ghosh, K. Glaesemann, A. W. Götz, J. Hammond, V. Helms, E. D. Hermes, K. Hirao, S. Hirata, M. Jacquelin, L. Jensen, B. G. Johnson, H. Jónsson, R. A. Kendall, M. Klemm, R. Kobayashi, V. Konkov, S. Krishnamoorthy, M. Krishnan, Z. Lin, R. D. Lins, R. J. Littlefield, A. J. Logsdail, K. Lopata, W. Ma, A. V. Marenich, J. Martin Del Campo, D. Mejia-Rodriguez, J. E. Moore, J. M. Mullin, T. Nakajima, D. R. Nascimento, J. A. Nichols, P. J. Nichols, J. Nieplocha, A. Otero-de-la-Roza, B. Palmer, A. Panyala, T. Pirojsirikul, B. Peng, R. Peverati, J. Pittner, L. Pollack, R. M. Richard, P. Sadayappan, G. C. Schatz, W. A. Shelton, D. W. Silverstein, D. M. A. Smith, T. A. Soares, D. Song, M. Swart, H. L. Taylor, G. S. Thomas, V. Tipparaju, D. G. Truhlar, K. Tsemekhman, T. Van Voorhis, Á. Vázquez-Mayagoitia, P. Verma, O. Villa, A. Vishnu, K. D. Vogiatzis, D. Wang, J. H. Weare, M. J. Williamson, T. L. Windus, K. Woliński, A. T. Wong, Q. Wu, C. Yang, Q. Yu, M. Zacharias, Z. Zhang, Y. Zhao and R. J. Harrison, *J. Chem. Phys.*, 2020, **152**, 184102.
22 M. J. Frisch, G. W. Trucks, H. B. Schlegel, G. E. Scuseria, M. A. Robb, J. R. Cheeseman, G. Scalmani, V. Barone, G. A. Petersson, H. Nakatsuji, X. Li, M. Caricato, A. V. Marenich, J. Bloino, B. G. Janesko, R. Gomperts, B. Mennucci, H. P. Hratchian, J. V. Ortiz, A. F. Izmaylov, L. Sonnenberg, D. Williams-Young, F. Ding, F. Lipparini, F. Egidi, J. Goings, B. Peng, A. Petrone, T. Henderson, D. Ranasinghe, V. G. Zakrzewski, J. Gao, N. Rega, G. Zheng, W. Liang, M. Hada, M. Ehara, K. Toyota, R. Fukuda, J. Hasegawa, M. Ishida, T. Nakajima, Y. Honda, O. Kitao, H. Nakai, T. Vreven, K. Throssell, J. A. Montgomery, Jr., J. E. Peralta, F. Ogliaro, M. J. Bearpark, J. J. Heyd, E. N. Brothers, K. N. Kudin, V. N. Staroverov, T. A. Keith, R. Kobayashi, J. Normand, K. Raghavachari, A. P. Rendell, J. C. Burant, S. S. Iyengar, J. Tomasi, M. Cossi, J. M. Millam, M. Klene, C. Adamo, R. Cammi, J. W. Ochterski, R. L. Martin, K. Morokuma, O. Farkas, J. B. Foresman and D. J. Fox, *GaussView 5.0*, Gaussian, Inc., Wallingford, CT, 2016.
23 M. D. Hanwell, D. E. Curtis, D. C. Lonie, T. Vandermeersch, E. Zurek and G. R. Hutchison, *J. Cheminf.*, 2012, **4**, 17.
24 *Avogadro: An Open-Source Molecular Builder and Visualization Tool, Version 1.2.0*, **https://Avogadro.cc/**.
25 H. Sakurai, T. Daiko, H. Sakane, T. Amaya and T. Hirao, *J. Am. Chem. Soc.*, 2005, **127**, 11580–11581.
26 A. Klamt and G. Schüürmann, *J. Chem. Soc., Perkin Trans. 2*, 1993, 799–805.
27 A. D. Becke, *J. Chem. Phys.*, 1993, **98**, 5648–5652.
28 C. Lee, W. Yang and R. G. Parr, *Phys. Rev. B: Condens. Matter Mater. Phys.*, 1988, **37**, 785–789.
29 R. L. Martin, *J. Chem. Phys.*, 2003, **118**, 4775–4777.
30 P. C. Meier, W. E. Morf, M. Läubli and W. Simon, *Anal. Chim. Acta*, 1984, **156**, 1–8.
31 R. Eugster, P. M. Gehrig, W. E. Morf, U. E. Spichiger and W. Simon, *Anal. Chem.*, 1991, **63**, 2285–2289.
32 H. A. Benesi and J. H. Hildebrand, *J. Am. Chem. Soc.*, 1949, **71**, 2703–2707.